

# UDRN: Unified Dimensional Reduction Neural Network for Feature Selection and Feature Projection <sup>★,★</sup>

Mr. Zelin Zang<sup>a,b,c,1</sup>, Yongjie Xu<sup>b,c</sup>, Yulan Geng<sup>b,c</sup>, Siyuan Li<sup>b,c</sup> and Prof Stan.Z Li<sup>b,c,\*</sup>

<sup>a</sup>Zhejiang University, Hangzhou, 310000, China

<sup>b</sup>Westlake University, AI Lab, School of Engineering, Hangzhou, 310000, China

<sup>c</sup>Westlake Institute for Advanced Study, Institute of Advanced Technology, Hangzhou, 310000, China

## ARTICLE INFO

### Keywords:

Dimensional Reduction  
High-dimensional Data Analysis  
Feature Selection  
Feature Projection

## ABSTRACT

Dimensional reduction (DR) maps high-dimensional data into a lower dimensions latent space with minimized defined optimization objectives. The DR method usually falls into feature selection (FS) and feature projection (FP). FS focuses on selecting a critical subset of dimensions but risks destroying the data distribution (structure). On the other hand, FP combines all the input features into lower dimensions space, aiming to maintain the data structure; but lacks interpretability and sparsity. FS and FP are traditionally incompatible categories; thus, they have not been unified into an amicable framework. We propose that the ideal DR approach combines both FS and FP into a unified end-to-end manifold learning framework, simultaneously performing fundamental feature discovery while maintaining the intrinsic relationships between data samples in the latent space. In this work, we develop a unified framework, Unified Dimensional Reduction Neural-network (UDRN), that integrates FS and FP in a compatible, end-to-end way. We improve the neural network structure by implementing FS and FP tasks separately using two stacked sub-networks. In addition, we designed data augmentation of the DR process to improve the generalization ability of the method when dealing with extensive feature datasets and designed loss functions that can cooperate with the data augmentation. Extensive experimental results on four image and four biological datasets, including very high-dimensional data, demonstrate the advantages of DRN over existing methods (FS, FP, and FS&FP pipeline), especially in downstream tasks such as classification and visualization.

## 1. Introduction

Dimensional reduction (DR) [1, 2] transforms data from a high-dimensional (h-dim) space into an intrinsic low-dimensional (l-dim) space with minimal loss of valid information. DR has the potential to combat dimensional catastrophes, so it is commonly used in files with large numbers of variables/features, such as signal processing [3], speech recognition [4], neuroinformatics [5], and bioinformatics [6].

Generally speaking, the ideal DR method is expected to have the following two *characteristics*: (1) **Structural maintainability**. DR reduces the data dimension while preserving important information from being corrupted. Under the manifold assumption, ensuring the local connectivity of data is the golden rule of structure-preservation. (2) **Sparse interpretability**. The DR often has super high dimensionality input data, and it is difficult to identify the presence of redundant features. Removing redundant features and highlighting important features can explain how DR works and guide data collection. In many scientific exploration fields, such as bioinformatics and neuroinformatics, DR is required to have both characteristics.

Unfortunately, the current DR approaches are unable to achieve the above *characteristics* based on a unified

framework. They often contain two incompatible branches: feature projection (FP) [7] and feature selection (FS) [8]. FP methods produce new variables obtained from the original features via an arbitrarily complex mapping, thus having better distinguish and structure-preserving performance. In contrast, FS methods with better interpretability allow the user to find an essential feature subset during the generalization phase of the model but often break the structure of the data by losing features [9, 10, 11].

Due to practical needs in areas such as biology, some researchers build a pipeline by splicing the FS and FP methods together to solve the above issues [12, 13]. However, these pipelines only achieve sub-optimal results due to two fatal issues: **Inconsistent optimization objective**. The stacked approach of FS and FP may introduce conflicting objectives, e.g., FS focuses on reconstruction error while FP focuses on distance/similarity preserving. **Weak generalizability**. FS and FP are mainly applied in scenarios with a huge number of features, where it is easy to fall into overfitting due to the relatively small number of samples. **Feature information leakage**. Almost all NN-based FS approaches take offline feature selection, implying that score optimization and subset selection are performed separately, resulting in FS not being embedded in the end-to-end network. When scoring optimization, much information about unimportant features that should be discarded is leaked into the network, affecting the performance of feature selection.

This paper designs an end-to-end NN-based model, Unified Dimensionality Reduction Neural-network (UDRN), to perform feature selection and projection (FS&FP) in a

<sup>\*</sup>This document is the results of the research project funded by the National Science Foundation.

<sup>\*\*</sup>The second title footnote which is a longer text matter to fill through the whole text width and overflow into another line in the footnotes area of the first page.

ORCID(s): 0000-0003-2831-5437 (Z. Zang)

unified framework. *To enhance the generalizability of the model*, we designed data augmentation methods (named FMH augmentation) applicable to FS and FP. The FMH augmentation improves the generalizability and stability of UDRN by generating new data points inside the manifold. We design a novel loss function based on the traditional structure-preserving loss function. The loss function is made compatible with data augmentation and feature selection. *To avoid the leakage of feature information*, we design FS network with a gate operation that *mask off* unimportant features during the training process, thus implementing online feature selection and enabling the following FP with selected features. To this end, the proposed UDRN selects a suitable feature subset and then maps it to the l-dim space to complete downstream tasks such as classification and visualization. This paper is a groundbreaking attempt to apply structure-preserving loss functions and data augmentation on FS&FP to the best of our knowledge.

Our contributions are summarized as follows:

- **Unified FS&FP problem and a novel neural network framework:** We propose the problem of FS&FP with a unified objective and design a neural network framework to solve this problem. The problem is widely needed in biology, genomics, and proteomics.
- **Novel data augmentation for FS&FP and corresponding loss functions:** We propose a novel structure-preserving loss function and online FMH augmentation to provide a consistent and generalizable objective function.
- **Extensive experiments and promising results:** We compare UDRN with state-of-the-art FS, FP, and FS&FP pipeline methods on ten datasets and a case study of the supervised scenarios.

## 2. Related Work

### 2.1. Feature Projection (FP)

In recent years, Numerous manifold-learning-based FP methods have been proposed. Some of the FP methods are based on the manifold assumption [14, 15], which states that a pattern of interest in data is a lower-dimensional manifold (or hyper-surface) residing in the high dimensional data space. When the data contains multiple manifolds, the geometric structure usually includes the local structure of neighboring points on each manifold and global relationships among different manifolds.

In terms of non-parametric models, the Isometric Mapping (ISOMAP) [16] and Locally Linear Embedding (LLE) [17] are classic ones, among others. Later developments include Hessian LLE (HLLE) [18], Modified LLE (MLLE) [19].

The t-Distributed Stochastic Neighbor Embedding (t-SNE) [20] and Uniform Manifold Approximation and Projection (UMAP) [21] are two popular methods for manifold learning-based NLDR, widely used for NLDR and visualization. The t-SNE improves the previous work of SNE [22] by using a long-tailed

*t*-distribution for the embedding layer [20]. The UMAP further introduces a global term added to the local neighborhood-based t-SNE to preserve the global structure.

In terms of parametric models, Topological Autoencoder (TAE) [23] imposes topological constraints [24] on top of the autoencoder architecture to preserve the topological structure of data. Deep Isometric Manifold Learning (DIMAL) [25] combines a deep learning framework with a multi-dimensional scaling (MDS) objective, which can be seen as a neural network version of MDS. DIMAL can learn a distance-preserving mapping to generate low-dimensional embeddings for a particular class of manifolds with sparse geodesic sampling.

### 2.2. Feature Selection (FS)

The FS methods have four categories [26]: (a) filter methods, which are independent of learning models; (b) wrapper methods, which rely on learning models for selection criteria; (c) embedder methods, which embed the feature selection into learning models to also achieve model fitting simultaneously; (d) hybrid approaches, which are a combination of more than one of the above three. Alternatively, We categorize these methods as supervised, semi-supervised, and unsupervised according to whether they need to use label information. Unsupervised feature selection has potentially broad applications because it requires no label information [27]; yet, it is also arguably more challenging due to the lack of labels to guide the identification of relevant features.

In terms of non-parametric models, LS [28] is a filter method that uses the nearest neighbor graph to model the local geometric structures of the data. By selecting the locally smoothest features, LS focuses on the local property yet neglects the global structure. Principal feature analysis (PFA) [29] utilizes the structure of the main components of a set of features to select the subset of relevant features. It is a wrapper method to optimize the PC coefficients, mainly focusing on globality. Multi-cluster feature selection (MCFS) [30] selects a subset of features to cover the multi-cluster structure of the data, where spectral analysis is used to find the inter-relationship between different components. In Unsupervised discriminative feature selection (UDFS) [31] the discriminative analysis method and  $\ell_{2,1}$  regularization is used to identify the valuable features. Nonnegative discriminative feature selection (NDFS) [32] select discriminative features by learning the cluster labels and feature selection matrix. The NDFS uses a nonnegative constraint on the class indicator to understand cluster labels and adopts an  $\ell_{2,1}$  limitation on the redundant features. IVFS [9] select useful features by preserving the pairwise distances, as well as topological patterns, of the complete data.

In terms of parametric models, NN-based methods are often used to solve feature selection problems for tabular data. Autoencoder Feature Selector (AEFS) [33] combines reconstruction loss and  $\ell_{2,1}$  regularization loss to obtain a subset of useful features on the weights of the encoder.

AEFS exploits both linear and nonlinear information in the features. The agnostic feature selection (AgnoS) [34] combines AE with different auxiliary tasks to design a range of feature selection methods. Such as, AgnoS-W: the  $\ell_{2,1}$  norm on the weights of the first layer of AE, AgnoS-G:  $\ell_{2,1}$  norm on the gradient of the encoder, and AgnoS-S:  $\ell_1$  norm on the slack variables that constitute the first layer of AE. Concrete Autoencoders (CAE) [10] replaces the first hidden layer of AE with a concrete selector layer, which is the relaxation of a discrete distribution called concrete distribution [35]. Fractal Autoencoders (FAE) [11] extends autoencoders by adding a one-to-one scoring layer. FAE uses a small sub-neural network for feature selection in an unsupervised fashion.

### 2.3. FS and FP (FS&FP) Pipelines

In biology, especially in single cell [13], genomics [36] and proteomics[37], pre-processing of data often requires complex pipelines, and FS and FP are two steps that are connected together. For example, in a single-cell dataset, studies [38] often employ differential expression (DE) analysis for FS and then map the selected features to lower-dimensional for downstream analysis (such as clustering, classification, and visualization).

In these fields, many FS methods and FP methods are experimented with the mentioned pipeline to expect good results[39]. However, the objective functions of FS methods and FP methods have different optimization goals, so the two unsupervised methods inevitably interfere with each other and thus with the performance of the output. Meanwhile, it would improve if the two interfering processes could be unified and optimized using an end-to-end framework and a unified loss function.

## 3. Problem Definition and Preliminaries

### 3.1. Problem Definition

We use bold uppercase characters for matrices (e.g.,  $\mathbf{A}$ ), bold lowercase characters for vectors (e.g.,  $\mathbf{a}$ ), and normal lowercase characters for scalars (e.g.,  $a$ ). Also, we represent the  $i$ -th element of vector  $\mathbf{a}$  as  $a_i$ , the  $i$ -th row of matrix  $\mathbf{A}$  as  $\mathbf{A}_{i*}$ , the  $j$ -th column of matrix  $\mathbf{A}$  as  $\mathbf{A}_{*j}$ , the  $(i, j)$ -th entry of matrix  $\mathbf{A}$  as  $A_{ij}$ , the transpose of  $\mathbf{A}$  as  $\mathbf{A}^T$ .

We introduce our proposed concept on the attributed graph to precisely describe our data augmentation and loss function and adapt it to a broader range of situations.

**Definition 2.1 (Attributed Graph).** Let graph  $\mathcal{G}(\mathcal{V}, \mathcal{E}, \mathcal{X})$  be an attributed graph(network). It's consists of - (1)  $\mathcal{V}$ : the set of nodes,  $n = |\mathcal{V}|$ , where  $n$  is the number of the nodes. (2)  $\mathcal{E}$ , the set of edges,  $e = |\mathcal{E}|$ , where  $e$  is the number of the edges. and (3)  $\mathcal{X} = [\mathbf{x}_1, \mathbf{x}_2, \dots, \mathbf{x}_n]$ : the set of node attributes (features), where  $\mathbf{x}_i \in \mathcal{R}^D$ ,  $D$  is the dimensional number of attribute.

With the definition of the attributed graph, we now define the FS&FP problem as follows.

**Definition 2.2 (FS&FP on Attributed Graph).** Given an attributed network  $\mathcal{G}(\mathcal{V}, \mathcal{E}, \mathcal{X})$ , the FS&FP on attributed graph

aims to: (a) select a subset of  $d$  features from the original  $D$ -dimensional feature space, and  $d \ll D$  and then (b) map the data with selected features  $\mathcal{X}^h$  to a latent space  $\mathcal{Z}$ . The obtained feature subsets and embedding results represent the original data as possible. Generally, we use  $k$ -NN graphs to build the edge structures in unsupervised contexts.

$$\mathcal{E} = \{(\mathbf{v}_i, \mathbf{v}_j) | \mathbf{v}_j \in \mathcal{N}^k(\mathbf{v}_i), \mathbf{v}_i \in \mathcal{V}\} \quad (1)$$

where  $\mathcal{N}(\mathbf{v}_i)$  is set of  $k$ -NN neighborhood of node  $\mathbf{v}_i$ . The advantage of using the graph description our method is that the scheme is easily compatible with supervised situations.

$$\mathcal{E} = \{(\mathbf{v}_i, \mathbf{v}_j) | \mathbf{v}_j \in \mathcal{N}^k(\mathbf{v}_i) \cap Y(\mathbf{v}_i), \mathbf{v}_i \in \mathcal{V}\} \quad (2)$$

where  $Y(\mathbf{v}_i)$  is the set of nodes with the same label as  $\mathbf{v}_i$ .

### 3.2. Preliminary: AE-based Feature Selection

AE-based FS methods add a superficial one-to-one layer between the input and hidden layers of AE to weigh the importance of each feature [33, 10, 11]. It is exploit the sparsity property of  $L_1$  regularization for the weights of this layer for FS. Then, AE-based FS is,

$$\min_{\mathcal{W}, f_\theta, g_\phi} \left\| \mathbf{x} - g_\phi(f_\theta(\mathbf{x}\mathcal{W})) \right\|_F^2 + \lambda_1 L_1(\mathbf{w}) \quad (3)$$

where  $\mathcal{W} = \text{Diag}(\mathbf{w})$ , and the  $\mathbf{w} \in \mathcal{R}^D$  is feature importance. The encoder  $f_\theta(\cdot)$  embeds the input data  $\mathbf{x}\mathcal{W}$  into a latent space, and the decoder  $g_\phi(\cdot)$  maps the latent space data back to the original space and calculates the reconstruction loss. The  $L_1$  loss leads to a decrease in  $\mathbf{w}$ , while the reconstruction loss increases the feature importance of important features, and the two losses act synergistically to guide important features to have higher scores.

The AE-based FS has been proven valid. However, the experiments indicate these methods are unsatisfactory in the following two aspects. (D1) **Leakage of unimportant feature information.** AE does not interrupt the forward propagation of any features during the training process but reduces the weights and eventually selects the essential features at the end of the algorithm optimization. The DR results obtained by such a scheme are not credible because of the mixed information of the discarded features. (D2) **Difficult to preserve the structure well in the latent space.** The AE-based approach focuses more on whether the selected features can reconstruct all components (including redundancy and noise) at the pixel level while less considering the essential structure of the data. Although AE is the most advanced FS method at present, we cannot use it as a baseline for FS&FP. In addition, less considering the structural information of the data destroy the discriminative performance of the method.

### 3.3. Preliminary: Node Similarly

To describe the relationship of nodes on the graph, we use Node Similarly (NS) [40] to fuse both structural and feature information for the metric.

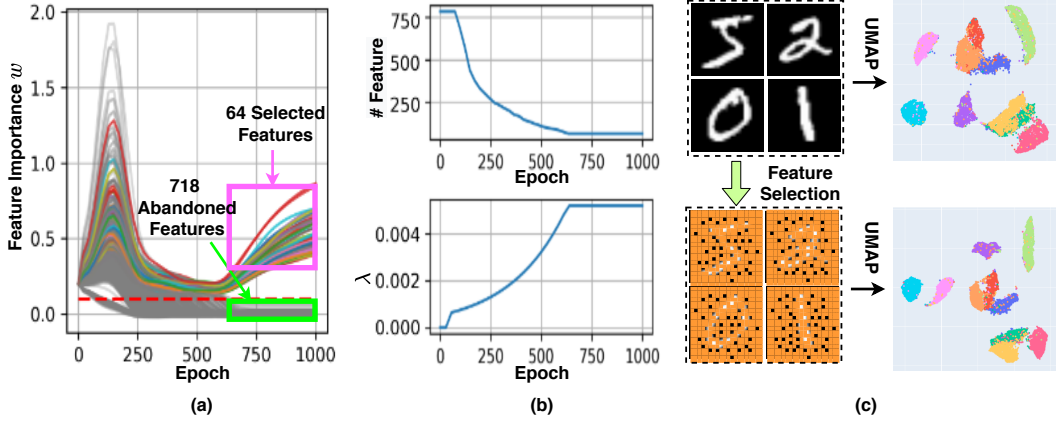


**Figure 1:** The framework of UDRN. UDRN consists: (a) FMH augmentation operation  $\tau$ , (b) feature selection (FS) network & feature projection (FP) network, (c) structure preservation loss function  $L_{tp}$ . The  $\tau$  generates new augmented graph  $\mathcal{G}'(\mathcal{V}', \mathcal{E}', \mathcal{X}')$  by Eq. (7). The FS network filter out unimportant features and map the data with selected features to high-dim embedding graph  $\mathcal{G}^h(\mathcal{V}', \mathcal{E}', \mathcal{Z}^h)$ ; FP network map the  $\mathcal{G}^h$  low-dim embedding graph  $\mathcal{G}'(\mathcal{V}', \mathcal{E}', \mathcal{Z}')$ . The  $L_{tp}$  train FS and FP network with an end-to-end loss function.

**Definition 2.3 (Node Similarly, NS, w.r.t.  $\mathcal{S}$ ).** Given an attributed network  $\mathcal{G}(\mathcal{V}, \mathcal{E}, \mathcal{X})$ , and a kernel function  $\kappa(\cdot, \cdot)$ , the node similarly is:

$$S_{ij}^G = \kappa(\mathbf{x}_i, \mathbf{x}_j) \quad (4)$$

The kernel function transforms the distance relationship between nodes into the similarity relationship and thus constructs the structure-preserving loss function. The frequently used kernel functions include Gaussian kernel [41]:

$$\kappa(\mathbf{x}_i, \mathbf{x}_j) = \exp\left(-\|\mathbf{x}_i - \mathbf{x}_j\|^2/2\sigma^2\right) \quad (5)$$

where  $\sigma$  is a scaling factor. another frequently used kernel functions is t-kernel [20]:

$$\kappa(\mathbf{x}_i, \mathbf{x}_j) = \left(1 + \|\mathbf{x}_i - \mathbf{x}_j\|^2/v\right)^{-\frac{v+1}{2}} \quad (6)$$

where  $v$  is freedom degree of t-distribution.

## 4. Methods

We aim to develop an end-to-end FS&FP method that leverages the beneficial properties of neural networks and data augmentation to improve the traditional pipeline (in Fig. 1).

### 4.1. Feature Meaning Holding Augmentation

Data augmentation is a commonly used NN training method for image classification and signal processing [42] and acts as a regularizer and helps reduce overfitting. We find that traditional image data augmentation schemes cannot directly apply to FS. The reason is that FS requires that the meaning of individual features is not destroyed by data augmentation. To this end, we give the requirements for Feature Meaning Holding Augmentation (FMH Augmentation).

**Definition 3.1 (FMH Augmentation, w.r.t  $\tau$ ).** Given an attributed network  $\mathcal{G}(\mathcal{V}, \mathcal{E}, \mathcal{X})$ , FMH Augmentation generates a corresponding augmented graph  $\mathcal{G}'(\mathcal{V}', \mathcal{E}', \mathcal{X}')$  and for detail:

$$\begin{aligned} \mathcal{V}' &= \{\mathbf{v}_1, \dots, \mathbf{v}_n, \mathbf{v}_1', \dots, \mathbf{v}_n'\} \\ \mathcal{E}' &= \{\mathcal{E} + \tilde{\mathcal{E}}' + \tilde{\mathcal{E}}''\} \\ \mathcal{X}' &= \{\mathbf{x}_1, \dots, \mathbf{x}_n, \tau(\mathbf{x}_1), \dots, \tau(\mathbf{x}_n)\} \end{aligned} \quad (7)$$

The augmented graph  $\mathcal{G}'$ 's node  $\mathcal{V}'$  contains: (1) original nodes  $\mathbf{v}_1, \dots, \mathbf{v}_n$ , and (2) augmented nodes  $\mathbf{v}_1', \dots, \mathbf{v}_n'$ , which corresponds to the original node one by one. The edges  $\mathcal{E}'$  contains: (1) original edges  $\mathcal{E}$ , which edges between the original nodes, (2) the inter-augmented nodes:  $\tilde{\mathcal{E}}' = \{(\mathbf{v}_1, \mathbf{v}_1'), \dots, (\mathbf{v}_n, \mathbf{v}_n')\}$ , and (3) intra-augmented edges  $\tilde{\mathcal{E}}''$ , which between the augmented nodes  $\tilde{\mathcal{E}}'' = (\mathbf{v}_i, \mathbf{v}_j) \rightarrow (\mathbf{v}_i', \mathbf{v}_j')$ . Three kinds of edges are qualitatively different and should be modeled separately. However, we focus on the nearest neighbor relationship depicted by the edge structure and model the three edge structures as homogeneous graphs for modeling convenience.

The FMH augmentation operator by fusing the local structure information and random distribution. Several FMH augmentations are as follows:

**(i) Uniform-type FMH augmentation (w.r.t  $\tau_U$ )** generates augmented data by linear combination, linear combination parameter  $r_u$  is sampled from the uniform distribution  $U(0, p_U)$ ,  $p_U$  is the hyperparameter.

$$\begin{aligned} \tau_U(\mathbf{x}) &= (1 - r_u) \cdot \mathbf{x} + r_u \cdot \tilde{\mathbf{x}}, \\ \tilde{\mathbf{x}} &\sim \mathcal{N}^k(\mathbf{x}), r_u \sim U(0, p_U) \end{aligned} \quad (8)$$

where  $\tilde{\mathbf{x}}$  is sampled from the attributes set of data  $\mathbf{x}$ 's  $k$ -NN neighborhood  $\mathcal{N}^k(\mathbf{x})$ .

**(ii) Bernoulli-type FMH augmentation (w.r.t  $\tau_B$ )** generates augmented data by directly substitutes some features

by there neighbor data's corresponding features, the probability of replacement  $b_j$  is sampled from the Bernoulli distribution  $B(p_B)$ , and  $p_B$  is the success probability of Bernoulli distribution.

$$\begin{aligned}\tau_B(\mathbf{x}) &= \mathbf{x} \circ \mathbf{b} + \tilde{\mathbf{x}} \circ (1 - \mathbf{b}), \tilde{\mathbf{x}} \sim \mathcal{N}^k(\mathbf{x}), \\ \mathbf{b} &= \{b_j | b_j \sim B(p_B), j \in \{1, \dots, \mathcal{D}\}\}\end{aligned}\quad (9)$$

where  $\circ$  is the hadamard product.

(iii) **Normal-type FMH augmentation (w.r.t  $\tau_N$ )** generates augmented data by adding some noise, noise parameters  $b_j$  is sampled from the normal distribution  $N(0, p_N)$ , and  $p_N$  are the standard deviation. The distance between neighboring sample features as a scaling factor to avoid destroying of single feature.

$$\begin{aligned}\tau_N(\mathbf{x}) &= \mathbf{x} + (\mathbf{x} - \tilde{\mathbf{x}}) \circ \mathbf{b}, \tilde{\mathbf{x}} \sim \mathcal{N}^k(\mathbf{v}), \\ \mathbf{b} &= \{b_j | r_j \sim N(0, p_N), j \in \{1, \dots, \mathcal{D}\}\}\end{aligned}\quad (10)$$

The FMH augmentation operators are applied online during network training, thus providing more randomness of the data and guaranteeing that the feature meaning does not change. We also discuss the effect of different data augmentation on feature selection.

## 4.2. FS Network and FP Network

We designed the FS network  $f_{\theta, \mathbf{w}}(\cdot)$  and the FP network  $g_{\phi}(\cdot)$ . The network  $f_{\theta, \mathbf{w}}(\cdot)$  learn the sparse feature subset *online* and then map the data with selected features into high dimensional embedding  $\mathcal{Z}^h$ ; and the FP network further maps  $\mathcal{Z}^h$  to low dimensional embedding  $\mathcal{Z}^l$ .

Most FS methods involve a *offline feature selection* strategy. It includes two steps: (a) all features are scored for importance using various objective functions; (2) the top-k essential features are selected. Such an offline scheme creates an obstacle to the unification of FS&FP because the model must select the exact subset of features during the training process before subsequent FP can be performed. Therefore, we designed the *online feature selection* network as follows:

$$\begin{aligned}\mathcal{X}^h &= m(\mathcal{X}') = \mathcal{X}' \cdot (\mathcal{W} \circ \mathbf{1}_{\mathcal{W} > \epsilon}) \\ \mathcal{Z}^h &= f_{\theta}(\mathcal{X}^h)\end{aligned}\quad (11)$$

where  $f_{\theta}(\cdot)$  is a MLP, the  $\mathcal{W} = \text{Diag}(\mathbf{w})$  is a feature importance matrix, the  $\mathbf{w} \in \mathbb{R}^D$  is the feature importance. The  $\epsilon$  is a hyperparameter threshold,  $\circ$  is Hadamard product, and the  $\mathbf{1}_{\mathcal{W} > \epsilon}$  is a gate layer to ensure the features with low importance score are not leakage to the latter network layer. The forward propagation of the FP network  $g_{\phi}(\cdot)$  is:

$$\mathcal{Z}^l = g_{\phi}(\mathcal{Z}^h). \quad (12)$$

The  $f_{\theta, \mathbf{w}}(\cdot)$  and  $g_{\phi}(\cdot)$  maps the data values  $\mathcal{X}'$  without changing the nodes  $\mathcal{V}'$  and edge  $\mathcal{E}'$ . Finally, we can get two graphs  $\mathcal{G}'(\mathcal{V}', \mathcal{E}', \mathcal{Z}^h)$  and  $\mathcal{G}'(\mathcal{V}', \mathcal{E}', \mathcal{Z}^l)$ .

## 4.3. Data Augmentation Compatible Loss

Next, we discuss how to design structure-preserving loss functions that are compatible with data augmentation and FS. The vanilla dimensional reduction (FP) loss function directly calculates the similarity of the input data  $\mathbf{X}$  and then minimizes the difference between the input space and the latent space using KL loss [20] or CE loss [41], respectively.

$$L_{\text{FP}} = \frac{1}{B^2} \sum_{i, j \in \mathcal{B}} \mathcal{S}_{ij}^X \log \mathcal{S}_{ij}^l + (1 - \mathcal{S}_{ij}^X) \log(1 - \mathcal{S}_{ij}^l) \quad (13)$$

where  $\mathcal{B} = \{1, 2, \dots, B\}$ ,  $B$  is the number of node in a batch. The  $\mathcal{S}_{ij}^X$  and  $\mathcal{S}_{ij}^l$  are the data similarity of node  $i$  and node  $j$  in the input space and latent space respectively. The  $\mathcal{S}_{ij}^X$  is often calculated before training the network by Eq. (4). And it is necessary to determine the parameter  $\sigma_i^*$  for every single node  $i$  by binary search under the hyper-parameter ‘n\_neighbors’ (or perplexity in t-SNE)  $p$  [41].

$$\sigma_i^* = \arg \min_{\sigma_i} \sum_j \{\exp(-\|\mathbf{x}_i - \mathbf{x}_j\|^2 / \sigma_i)\} - \log_2(p) \quad (14)$$

Unfortunately, the above loss function is not compatible with our framework. Firstly, our data augmentation and FS layer fundamentally change the distribution of input data, thus making it impossible to efficiently precompute  $\mathcal{S}_{ij}^X$ . Secondly, even without considering the computational efficiency online computation of  $\mathcal{S}_{ij}^X$  is prone to crash due to the unstable learning target. The main requirements of proposed loss function are as follows:

- (r1) **Consistent objective to perform FS&FP:** consistent objective to avoid the performance loss of FS and FP processes and to obtain better results.
- (r2) **Compatible FS and data augmentation:** avoiding abrupt changes in the loss function due to removing certain features or mixing certain features.
- (r3) **Focus on structural information preserving:** avoid over-focusing on individual features of the input data (e.g., reconstruction-based methods), as noise and useless information may be present in the features.

To meet the above requirements, we design data augmentation compatible structure-preserving loss functions  $L_{\text{tp}}$  by combining high dimensional node similarity  $\tilde{\mathcal{S}}^h$ , low dimensional node similarity  $\mathcal{S}^l$  and graph structures  $\mathcal{E}'$  (in Fig. 2). We expect the FS network to map the input features perturbed by the data augmentation and data selection layers to a stable high-dimensional latent space, and then the next FP network maps the high-dimensional latent space to a lower dimension.

Data augmentation essentially provides a stronger data prior that the augmented data has similar semantics to the original data and should be mapped to similar locations in the latent space. To make better use of this prior, we design

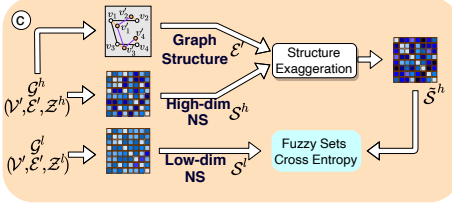


**Figure 2:** Framework of calculating  $L_{tp}$ . (1) abstract structure  $\mathcal{E}'$ . (2) use  $\mathcal{E}'$  to exaggerate the high-dimensional NS  $S^h$ . (3) calculate  $L_{tp}$  by applying fuzzy set cross-entropy to  $\tilde{S}^h$  and  $S^l$ .

the manifold exaggeration  $E(S_{ij}^h, \mathcal{E}')$ :

$$\begin{aligned} \tilde{S}_{ij}^h &= E(S_{ij}^h, \mathcal{E}') \\ &= \begin{cases} S_{ij}^h \exp(1 - \beta) & \text{if } (\mathbf{v}_i, \mathbf{v}_j) \in \mathcal{E}' \\ S_{ij}^h \exp(1 + \beta) & \text{otherwise} \end{cases} \end{aligned} \quad (15)$$

where  $\beta > 0$  is a robust hyperparameters. The idea of manifold exaggeration comes from the simple idea of pulling in nearest-neighbour nodes and pushing out non-nearest-neighbour nodes in dimensional reduction process. Such a push-pull operation is based on a given structure  $\mathcal{E}'$  and therefore incrementally guide the our UDRN to maintain structural information during FS&FP.

The loss function  $L_{tp}$  is as the form of fuzzy sets cross entropy [41] (two-way divergency in [43]):

$$L_{tp} = \frac{1}{B^2} \sum_{i,j \in B} \tilde{S}_{ij}^h \log S_{ij}^l + (1 - \tilde{S}_{ij}^h) \log(1 - S_{ij}^l) \quad (16)$$

$L_{tp}$  overcomes the weaknesses of the vanilla DR loss. First,  $L_{tp}$  does not directly use the features in the input space to compute the similarity so it is not directly affected by data augmentation and feature selection. Secondly, it is no longer necessary to compute the specificity  $\sigma$  for each node and has an advantage in computational complexity.

Finally, the loss function of unsupervised UDRN is :

$$\min_{w, \theta, \phi} L_{tp} + \lambda L_r, \quad L_r = \|\mathbf{w}\|_1, \quad (17)$$

where  $\lambda$  is hyperparameter. To select a specific features number, we give  $\lambda$  a small initial value, and then slowly increase  $\lambda$  until the features number satisfies the requirements.

#### 4.4. Pseudocode

Algorithm. 1 shows how to train our model and how to obtain the selected features.

### 5. Experiments

#### 5.1. Details of Dataset and Compared Methods

**Details of Dataset:** We used four image datasets (COIL20, Mnist, KMnist, EMnist) and six biological datasets (Activity, HCL, Gast, and MCA). The details of the dataset are Table 1. Unlike CAE [10] and FAE [11], we do not downsample the dataset because of the computational time.

#### Algorithm 1 The DRN algorithm

**Input:** Data:  $\mathcal{G}_{all}(\mathcal{V}, \mathcal{E}, \mathcal{X})$ , Learning rate:  $\alpha$ , Epochs:  $E$ , Batch size:  $B$ , Network:  $f_{\theta, w}, g_{\phi}$ , loss weights:  $\lambda$ ,

**Output:** Selected Features:  $\mathcal{X}^h$ . FS&FP Embedding:  $\mathcal{Z}_{all}^l$ .

```

1: Let  $t = 0$ .
2: while  $i = 0; i < E; i++$  do
3:   while  $b = 0; b < [|\mathcal{X}|/B]; b++$  do
4:      $\mathcal{G}(\mathcal{V}, \mathcal{E}, \mathcal{X}) \leftarrow \text{Sampling}(\mathcal{G}_{all}(\mathcal{V}, \mathcal{E}, \mathcal{X}), b)$ ;
       # Sample a batch data
5:      $\mathcal{G}'(\mathcal{V}', \mathcal{E}', \mathcal{X}') \leftarrow \text{Augment}(\mathcal{G}(\mathcal{V}, \mathcal{E}, \mathcal{X}))$  by Eq. (7);
       # Data augmentation
6:      $\mathcal{X}^h = m(\mathcal{X}')$  by Eq. (11);
       # Select the features
7:      $\mathcal{G}^h(\mathcal{V}', \mathcal{E}', \mathcal{Z}^h) \leftarrow f(\mathcal{G}'(\mathcal{V}', \mathcal{E}', \mathcal{X}^h))$  by Eq. (11);
       # Map to high dimension space
8:      $\mathcal{G}^l(\mathcal{V}', \mathcal{E}', \mathcal{Z}^l) \leftarrow g(\mathcal{G}^h(\mathcal{V}', \mathcal{E}', \mathcal{Z}^h))$  by Eq. (12);
       # Map to low dimension space
9:      $\tilde{S}_{ij}^h \leftarrow S(\mathcal{G}^h(\mathcal{V}', \mathcal{E}', \mathcal{Z}^h))$ ; # Cal high dim similarity
10:     $S_{ij}^l \leftarrow S(\mathcal{G}^l(\mathcal{V}', \mathcal{E}', \mathcal{Z}^l))$ ; # Cal low dim similarity
11:     $\tilde{S}_{ij}^h \leftarrow E(S_{ij}^h, \mathcal{E}')$ ; # Manifold exaggeration
12:     $\mathcal{L}_{tp} \leftarrow L_{tp}(\tilde{S}_{ij}^h, S_{ij}^l)$  by Eq. (16); # Cal. the structural
       preservation loss
13:     $\mathcal{L}_1 \leftarrow L_1(\mathbf{w})$  by Eq. (17); # Cal. the L1 loss
14:     $\theta \leftarrow \theta - \alpha \frac{\partial \mathcal{L}_{tp}}{\partial \theta}, \phi \leftarrow \phi - \alpha \frac{\partial \mathcal{L}_{tp}}{\partial \phi}, \mathbf{w} \leftarrow \mathbf{w} - \alpha (\frac{\partial \mathcal{L}_{tp}}{\partial \mathbf{w}} + \frac{\partial \mathcal{L}_1}{\partial \mathbf{w}})$ 
       # Update the parameters
15:  end while
16: end while
17:  $\mathcal{X}^h \leftarrow m(\mathcal{G}_{all}(\mathcal{V}, \mathcal{E}, \mathcal{X}))$ ; # Select the features
18:  $\mathcal{Z}_{all}^l \leftarrow f(g(\mathcal{G}_{all}(\mathcal{V}, \mathcal{E}, \mathcal{X})))$ ;
       # Cal. the embedding result

```

We consider performance on large datasets as an essential evaluation metric.

**Compared Methods:** To demonstrate the advantages of UDRN, we have compared it not only with the FS method and the FP method alone but also with FS and FP pipeline methods. We classify all compared methods according to non-NN-based methods and NN-based methods. The compared Non-NN-based FS methods include LS [28], MCFS [44], NDFS [45], and IVFS [9]. The compared NN-based FS methods include AEFS [33], CAE [10], FAE [46], and QS [47]. The compared Non-NN-based FP methods include tSNE [48], UMAP [21]. The compared NN-based FP methods include GRAE [49], IVIS [50] and Parametric UMAP (PUMAP) [51].

We used the grid search method to determine the optimal parameters for all the baseline methods. The search space for each method is in Table. 2.

#### 5.2. Experimental Setup

We initialize the weights of the FS layer to  $\mathcal{W} = 0.2$  and initialize the other NN with the Kaiming initializer. We adopt the AdamW optimizer [52] with learning rate of 0.001. All experiments use a fixed MLP network structure,

**Table 1**  
Statistics of datasets.

	Dataset	#Sample	#Feature	#Class	Link
Image Data	Coil20	1440	16384	20	<a href="https://www.cs.columbia.edu/CAVE/software/softlib/coil-20.php">https://www.cs.columbia.edu/CAVE/software/softlib/coil-20.php</a>
	KMnist	60,000	784	10	<a href="https://pytorch.org/vision/stable/index.html">https://pytorch.org/vision/stable/index.html</a>
	Mnist	60,000	784	10	<a href="https://pytorch.org/vision/stable/index.html">https://pytorch.org/vision/stable/index.html</a>
	EMnist	731,668	784	10	<a href="https://pytorch.org/vision/stable/index.html">https://pytorch.org/vision/stable/index.html</a>
Biological Data	Activity	5,744	561	6	<a href="https://www.kaggle.com/uciml/human-activity-recognition-with-smartphones">https://www.kaggle.com/uciml/human-activity-recognition-with-smartphones</a>
	GAST	10,629	1457	12	<a href="https://www.ncbi.nlm.nih.gov/pmc/articles/PMC4643992/">https://www.ncbi.nlm.nih.gov/pmc/articles/PMC4643992/</a>
	MCA	30,000	9119	52	<a href="http://bis.zju.edu.cn/MCA/">http://bis.zju.edu.cn/MCA/</a>
	HCL	280,000	3037	93	<a href="https://figshare.com/articles/dataset/HCL_DGE_Data/7235471">https://figshare.com/articles/dataset/HCL_DGE_Data/7235471</a>

**Table 2**  
Details of grid search.

Methods	Search Space	Note
LS	$C \in [5, 10, 15, 20, 25, 30, 35, 40, 45, 50]$	$C \rightarrow$ cluster range
MCFS	$C \in [5, 10, 15, 20, 25, 30, 35, 40, 45, 50]$	$C \rightarrow$ cluster range
NDFS	$A \in [1, 1.5, 2], BETA \in [0.5, 1, 2], C \in [5, 15, 25]$	$A \rightarrow \alpha, C \rightarrow$ cluster range
IVFS	$T \in [D//10, D//20, D//50, D//80]$	$T \rightarrow$ tilde sample range, $D \rightarrow$ data shape
AEFS	$A \in [0.1, 0.2, 0.5], E \in [500, 1000, 2000]$	$A \rightarrow \alpha, E \rightarrow$ epoch
CAE	$B \in [256, 512], LR \in [0.01, 0.1, 1], DR \in [0, 0.5, 0.8]$	$B \rightarrow$ batch, $LR \rightarrow$ learning rate, $DR \rightarrow$ dropout
FAE	$B \in [128, 256, 512], E \in [500, 1000, 2000]$	$B \rightarrow$ batch, $E \rightarrow$ epoch
QS	$EP \in [2, 5, 10, 13, 20, 25], Z \in [0.1, 0.2, 0.3, 0.4, 0.5]$	$EP \rightarrow \epsilon, Z \rightarrow \zeta$

$f_{\theta, \mathbf{w}}$ : [-1, 500, 300, 80],  $g_{\phi}$ : [80, 500, 2], where -1 is the features number of the dataset. To make UDRN select a specified number of features, we set an adaptive  $\lambda$ . At the beginning of 300 epochs, the  $\lambda = 0$  model, and then  $\lambda = L_r/0.1\|\mathbf{w}\|_1$  and grow by 0.5% until the number of features meet the requirements. For all experiments  $\beta = 0.01$ . For the experiments in Table 3 to Table 6, we used Bernoulli-type FMH augmentation and set  $p_B = 0.4$ . For a fair comparison, we select features and train the ET tree on the training set (80% data), select the best hyperparameters on the validation set (10%), and report the results on the test set (10%).

### 5.3. Case Study

The Mnist dataset is selected to illustrate how UDRN works (Fig. 3). **FS prosessing.** At the beginning of training, because  $\mathcal{W} = 0.2$ , the network accepts all features of the data. But due to the constraint of  $L1$ ,  $\mathcal{W}$  gradually becomes smaller. Meanwhile, for the important features  $\mathcal{W}$  the getting smaller affects the structure maintenance, so eventually the  $L1$  loss and  $L_{tp}$  reach the balance to elect the important features (in Fig. 3(a) and (b)).

**FS & structure-preservation.** We expect the FS of UDRN to affect the local and global structure of the data as little as possible, which is the original intention of using the unified loss function for both FS and FP tasks. Based on the difference between the original features and the selected features in the Mnist data, we found that humans

can easily recognize the numbers in the images based on the selected features, indicating that our FS did not destroy the recognition of the images (in Fig. 3(c)). Meanwhile, we used UMAP to map the two data and found that the inter-cluster relationship did not change due to FS.

### 5.4. Comparison with FS methods

This section compares the performance with the unsupervised FS methods. The comparison includes discriminative and structure-preservation performance for a more comprehensive evaluation.

**Discriminative performance.** The discrimination performance compares the performance of the FS methods in classification tasks. Following CAE [10] and FAE [46], we use the ET tree classifier to evaluate the discriminative performance. For a fair comparison, 64 features are selected for all methods. The means and standard deviations of the accuracy are shown in Table. 3 and Table. 4. For a more extensive comparison, we compare the cases of selecting [16, 32, 64, 128, 256, 512] features. The comparison results are shown in Fig. 4.

**Analysis:** The conclusions are as follows: (a) In general, NN-based methods are superior to other methods. Among the NN-based methods, UDRN has the best results. UDRN has an advantage in all nine datasets. In addition, UDRN outperformed the second-best method by 1% in six datasets. (b) UDRN has more advantages in data with more features,

**Table 3**

Discriminative performance (classification accuracy) comparison with FS methods in image datasets; best result are shown in **bold**; results with clear advantage are shown in underline.

	LS	MCFS	NDFS	IVFS	AEFS	CAE	FAE	QS	UDRN
Coil20	21.0±0.6	34.0±1.3	8.1±1.5	98.6±0.7	99.3±0.2	97.7±0.7	—	98.0±0.5	<b>99.4±0.2(↑0.1)</b>
MNIST	17.0±0.1	76.0±0.4	90.4±0.6	42.4±0.1	86.4±0.3	92.1±0.2	69.9±0.4	93.2±0.2	<b>94.0±0.3(↑0.8)</b>
KMNIST	20.1±0.2	64.0±0.5	83.9±0.3	82.4±0.5	85.6±0.4	88.0±0.3	74.6±0.2	85.9±0.3	<b>89.6±0.4(↑1.6)</b>
EMNIST	7.9±0.1	43.6±0.9	64.3±0.6	42.5±0.3	65.6±0.4	63.9±0.3	50.0±0.3	68.0±0.3	<b>71.1±0.5(↑3.1)</b>
Average	16.5±0.2	54.4±0.6	61.7±0.8	66.5±0.5	84.2±0.3	85.4±0.4	64.8±0.3	86.2±0.3	<b>88.5±0.4(↑2.2)</b>

**Table 4**

Discriminative performance (classification accuracy) comparison with FS methods in biology datasets, best result are shown in **bold**; results with clear advantage are shown in underline.

	LS	MCFS	NDFS	IVFS	AEFS	CAE	FAE	QS	UDRN
Activity	92.3±0.3	42.4±1.8	48.5±3.8	95.8±0.3	96.9±0.2	98.0±0.1	74.8±0.8	97.4±0.2	<b>98.6±0.3(↑0.6)</b>
HCL	23.6±0.2	7.2 ±0.5	09.2±0.2	21.8±0.2	24.7±0.2	28.5±0.1	33.0±0.2	56.7±0.3	<b>62.0±0.2(↑5.3)</b>
Gast	68.9±0.5	42.1±3.6	44.4±1.6	73.9±0.6	73.6±0.6	89.1±0.3	81.0±0.3	86.8±0.6	<b>89.4±0.4(↑2.6)</b>
MCA	19.5±0.2	24.5±0.1	56.8±0.6	27.0±0.1	28.6±0.2	66.8±0.2	32.8±0.2	64.3±0.4	<b>77.8±0.4(↑13.5)</b>
Average	42.4±0.3	31.9±1.2	44.6±1.4	52.2±0.3	57.8±0.3	69.2±0.2	54.3±0.4	74.6±0.3	<b>79.7±0.3(↑5.1)</b>

for example, in data sets with more than 1000 features (as datasets in Table. 4), UDRN has more obvious advantages.

**Structure-preservation performance.** In the unsupervised case, the Structure-preservation performance tests whether the FS process breaks the neighborhood relationship of the original data. We use the nearest neighbor structure matching degree (SMD), a sampling-based structure metric for evaluation.

$$SMD = \frac{1}{k|\mathcal{V}|} \sum_{i \in \mathcal{X}, j \in \mathcal{N}^k(i)} |r_{i,j}^{\mathcal{X}} - r_{i,j}^{\mathcal{X}^h}| \quad (18)$$

where the  $r_{i,j}^{\mathcal{X}}$  and  $r_{i,j}^{\mathcal{X}^h}$  are the neighborhood ranking of  $v_j$  in  $v_i$  in the input and latent space. The results of six datasets are shown in Table 5.

**Analysis:** The conclusions are as follows: (a) The NN-based approach concentrates on reconstructing all input features and may not well-preserving the structure of selected features. (b) Many non-NN-based methods design objective functions based on structure retention and achieve suboptimal performance. The reason is that UDRN uses data augmentation and designs a loss function compatible with data augmentation, so it can better restrain the overfitting problem and achieve better structure preservation performance.

## 5.5. Comparison with FP methods

This section compares the discriminative performance with the baseline FP methods.

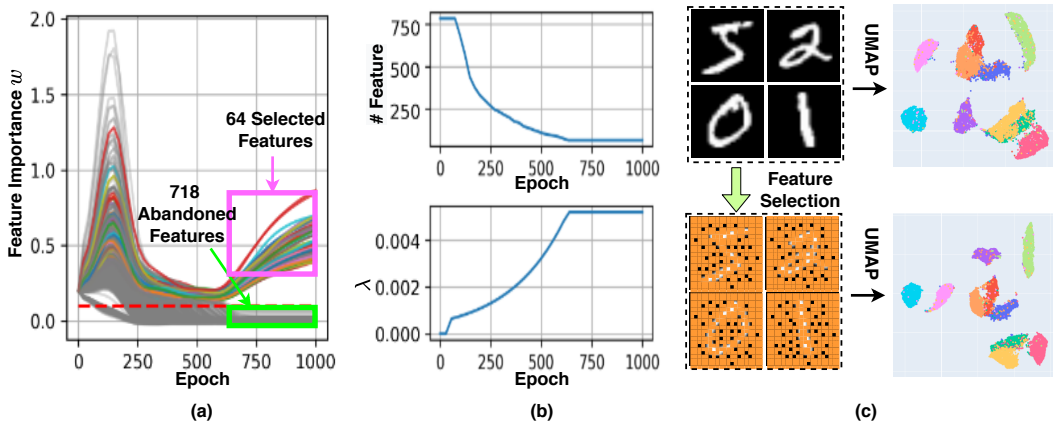


**Figure 3:** Case Study. (a) Variation plot of feature importance during training. Curves show the change in feature importance: colored curves (final selected features); gray curves (final discarded features). (b) Variation plot of the number of essential features ( $w_f > \tau$ ) and loss function weights  $\lambda$  during training. (c) UMAP Visualization of all features and the selected features.

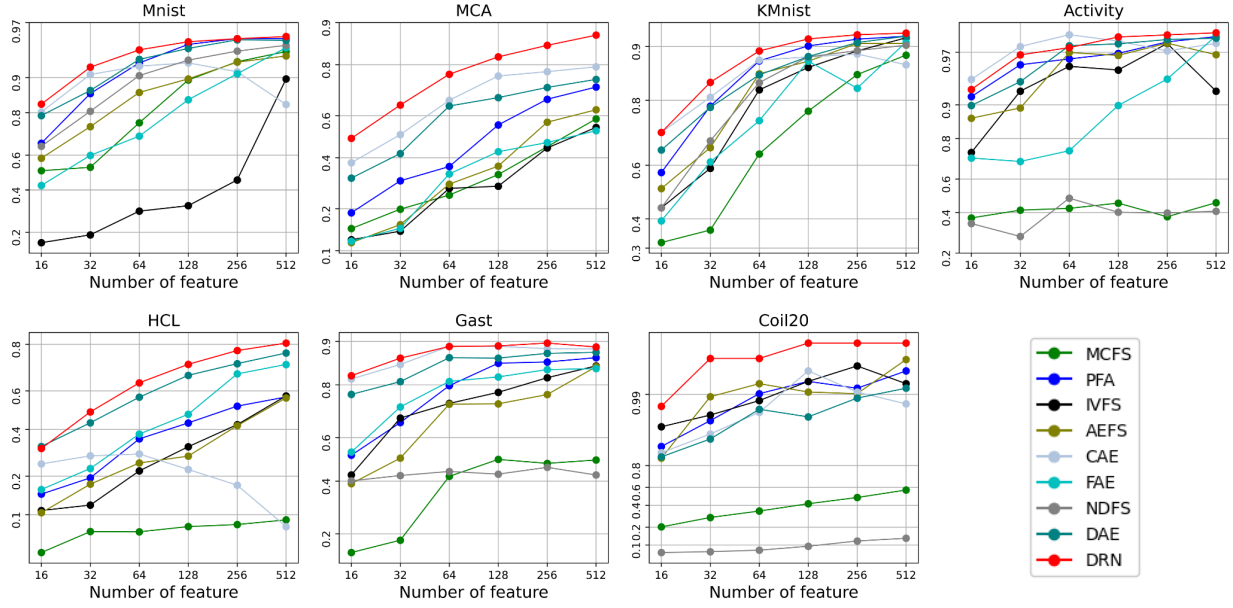


**Figure 4:** Classification accuracy with selected features. The horizontal coordinate represents the number of selected features and the vertical coordinate is the ACC of classification.

**Table 5**

Structure-preserving performance (SMD) comparison; best result are shown in **bold**.

	LS	IVFS	AEFS	CAE	FAE	UDRN
Mnist	17.0	86.9	59.6	42.7	46.8	<b>89.9</b>
KMNist	27.6	86.9	63.2	61.4	49.5	<b>88.3</b>
Activity	43.1	81.9	50.5	44.7	53.5	<b>99.9</b>
HCL	11.9	22.1	11.5	10.4	13.6	<b>27.8</b>
Gast	35.2	39.0	27.0	15.8	31.2	<b>48.2</b>
MCA	16.5	21.0	16.7	13.7	16.6	<b>26.9</b>

We disable the FS layer by setting  $\lambda = 0$  and project all the features into latent space for a fair comparison. Similar to sec. 5.4, we evaluate the discriminative performance by the accuracy of the ET tree classifier. The other settings are the same as sec. 5.4. The comparison results are in Table 6.

**Analysis:** Conclusions are as follows: (a) Except for UDRN, the performance of NN-based methods is inferior to that of non-NN methods. UDRN is not only optimal among all NN-based methods but also superior to non-NN-based methods. The results are consistent with those in [7]. (b) NN-based FP methods are challenging to train because the network parameters need to be optimized rather than the low-dimensional representations. Interestingly, UDRN can solve the training problem of FP networks through data augmentation and novel loss functions.

## 5.6. Visualization Comparison with FS&FP Pipeline

In application areas such as biology, many articles combine FP and FS methods for data analysis because the data contain many noisy features [53, 12]. We have discussed

**Table 6**

Discriminative performance comparison with FP methods; best result are shown in **bold**.

	tSNE	UMAP	GRAE	IVIS	PUMAP	UDRN
MNIST	<b>95.9</b>	94.5	77.2	68.3	94.2	<b>95.9</b>
KMNIST	<b>95.9</b>	93.8	85.4	72.8	91.5	94.7
Activity	92.0	91.9	88.9	82.1	90.0	<b>92.6</b>
HCL	58.4	44.9	53.1	53.3	51.4	<b>91.7</b>
Gast	69.5	62.7	90.1	76.4	64.5	<b>94.8</b>
MCA	51.5	41.3	83.6	66.7	46.6	<b>90.9</b>

the performance impact of these approaches in sec 2. Since we are the first to propose the concept of unifying FP and FS, we can only compare UDRN with FS&FP Pipeline. The advantages of UDRN can be demonstrated by visualization. Based on the experimental results shown in sec.5.4 and sec.5.5, we choose one FP method (UMAP) and multiple FS methods (IVFS, CAE, and QS) to combine. The visualization results are shown in Fig. 5).

**Analysis:** The conclusions are as follows: (a) When using all features, UMAP and UDRN can clearly show the structure, although different in detail. (b) When selecting fewer features, the compared methods can not guarantee the stability of the data's structure. For example, the embedding of features selected by IVFS is different from the embedding of the original features. (c) UDRN is very good at producing stable embeddings with only a small number of features due to the uniform loss function and data augmentation. The UDRN performs significantly better than the pipeline method from the visualization point of view.

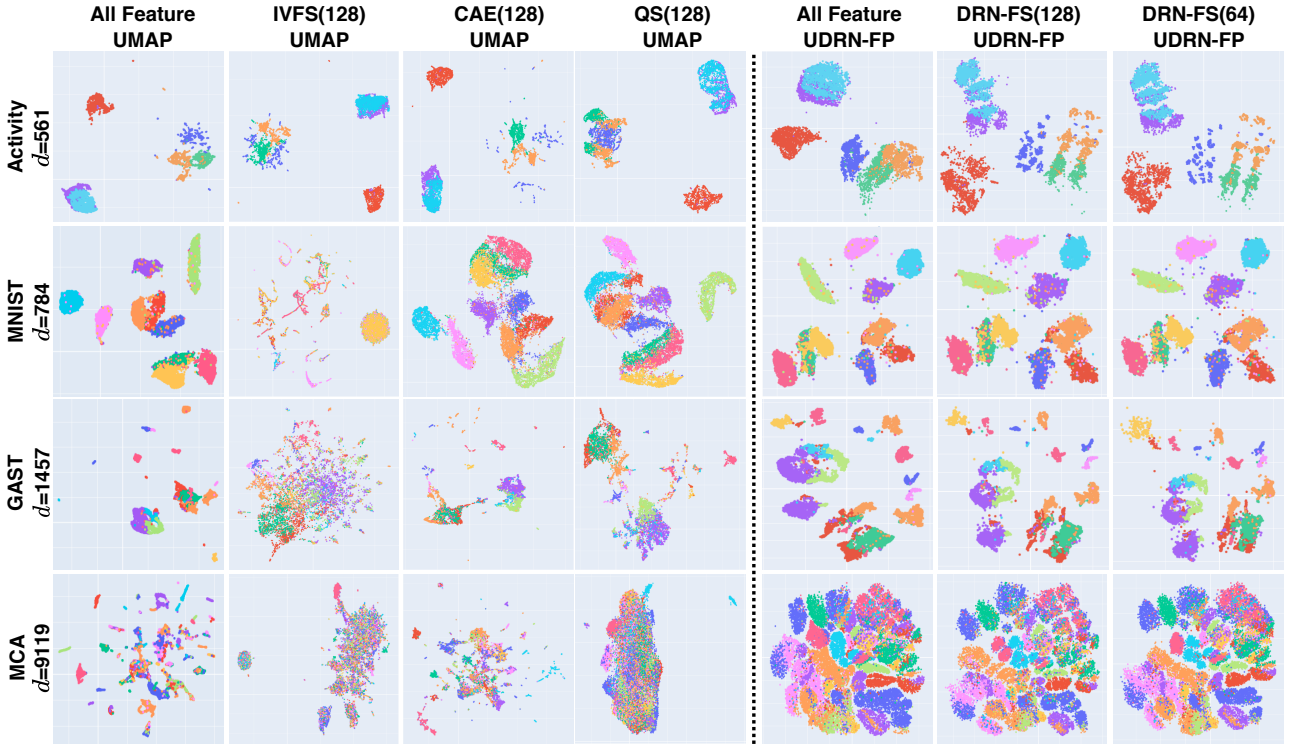


**Figure 5:** Visualization comparison with FS&FP pipeline. Each row represents a dataset. Each column represents a method: FS method (number of selected features) FP method, UDRN-FS and UDRN-FP are the features section and features projection of UDRN.

**Table 7**

Ablation study. The SVM classification accuracy on training set with different data augmentation hyperparameters. 0.0 means without the data augmentation.

	0.0	0.5	1.0	1.5	2.0	2.5	3.0
Mnist	95.3	97.2	96.9	97.1	97.4	<b>97.6</b>	96.3
KMnist	71.6	72.4	72.9	72.8	<b>73.2</b>	73.1	73.1
Gast10k	53.6	53.8	52.9	52.1	54.0	<b>54.4</b>	52.2
MCA	60.9	61.8	61.5	61.6	<b>62.0</b>	60.8	61.5
HCL	72.1	77.2	76.1	<b>77.9</b>	77.6	75.6	76.9
Average	71.1	72.5	72.2	72.4	72.8	72.4	72.1

## 5.7. Parameter Analysis

We analyze the effect of FMH Augmentation's hyperparameters and discuss the stability of the hyperparameters. We followed the sec. 5.4's setup and tested on the Mnist, EMnist, KMnist, HCL, MCA, and Gast datasets. (average ACC is in Table. 7).

**Analysis:** The conclusions are as follows: (1) FMH augmentation significantly enhances UDRN. Using any data augmentations can dramatically improve the method's performance. (2) The parameters of data augmentation have a relatively small impact on the algorithm, and in short, Normal-type FMH has a relative advantage. In general, the parameters of the FMH augmentation are very stable.

## 5.8. Ablation Study

We designed ablation experiments to demonstrate the effectiveness of UDRN. **Ablation 1:(w/o  $\tau$ ):** First, we remove the FMH data augmentation  $\tau$  and train the model directly using  $\mathcal{G}(\mathcal{V}, \mathcal{E}, \mathcal{X})$ . **Ablation 2 (w/o  $L_{tp}$ ):** Second, we remove Data Augmentation Compatible Loss  $L_{tp}$  and train the model directly using  $L_{FP}$ . **Ablation 3 (w/o  $\tau$ & $L_{tp}$ ):** Finally, we fuse the two changes of A1 and A2 together. The results of ablation experiments are in Table 8.

**Analysis:** The conclusions are as follows: (1) Removing either of the two operations alone brings a performance degradation, with the degradation from the loss function being more pronounced. (2) Both FMH data augmentation  $\tau$  and Data Augmentation Compatible Loss  $L_{tp}$  are very important and need to work together to improve the performance of the model. (3) The proposed loss function aims to be compatible with data augmentation and becomes a unified whole with data augmentation, so it should be used simultaneously.

## 5.9. Supervised UDRN (S-UDRN)

UDRN is well compatible with both supervised and unsupervised cases and only needs to consider whether supervised information is available when constructing the graph structure (in Eq. (1) and Eq. (2)). We chose a gut flora dataset to test UDRN under supervised scenarios. Since the gut flora dataset has few features associated with the labels, UDRN is needed to select highly relevant features from all the labels and complete the FP (in Fig. 6).

**Table 8**  
Ablation study of UDRN.

	Mnist	EMnist	KMnist	HCL	MCA
UDRN	<b>94.0</b>	<b>71.1</b>	<b>89.6</b>	<b>62.0</b>	<b>77.8</b>
w/o $\tau$	91.5	64.7	84.7	45.2	45.5
w/o $L_{tp}$	87.3	63.3	85.2	35.8	56.2
w/o $\tau$ & $L_{tp}$	82.5	61.8	82.3	31.6	42.1

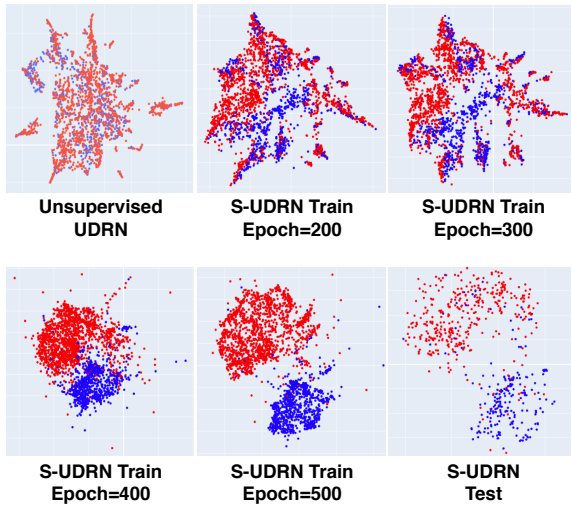


**Figure 6:** Visualization of unsupervised UDRN (UDRN) and supervised UDRN (S-UDRN). The proposed UDRN method is also compatible with the supervised case, and perform FS&FP based on data labels or other prior knowledge.

**Analysis:** The conclusions are as follows: (a) The dataset contains many useless features such that the unsupervised scheme is unable to distinguish classes. (b) Our UDRN approach can learn to distinguish labeled features based on a modified graph structure (based on labels), while at the same time, the intra-class manifold structure embedding does not receive influence.

## 6. Conclusion

We developed an integrated method for feature selection (FS) and feature projection (FP) with the help of neural networks named Unified Dimensional Reduction Neural-networks (UDRN). UDRN handles FS and FP tasks end-to-end with a unified loss function. UDRN is compatible with both supervised and unsupervised settings. We demonstrate the effectiveness and sophistication of UDRN by working with state-of-the-art FS, FP, and FS&FP pipeline methods.

## CRediT authorship contribution statement

**Stan.Z Li:** Conceptualization of this study, Methodology.

## References

- [1] S. Ayesha, M. K. Hanif, R. Talib, Overview and comparative study of dimensionality reduction techniques for high dimensional data, *Information Fusion* 59 (2020) 44–58.
- [2] S. Z. Li, Z. Zang, L. Wu, Deep manifold transformation for dimension reduction, *arXiv* (2020).
- [3] B. Chen, L. Chen, Y. Chen, Efficient ant colony optimization for image feature selection, *Signal processing* 93 (2013) 1566–1576.
- [4] Z.-T. Liu, M. Wu, W.-H. Cao, J.-W. Mao, J.-P. Xu, G.-Z. Tan, Speech emotion recognition based on feature selection and extreme learning machine decision tree, *Neurocomputing* 273 (2018) 271–280.
- [5] J. Deraeve, W. H. Alexander, Fast, accurate, and stable feature selection using neural networks, *Neuroinformatics* 16 (2018) 253–268.
- [6] B. Remeseiro, V. Bolon-Canedo, A review of feature selection methods in medical applications, *Computers in biology and medicine* 112 (2019) 103375.
- [7] J. Xia, Y. Zhang, J. Song, Y. Chen, Y. Wang, S. Liu, Revisiting dimensionality reduction techniques for visual cluster analysis: An empirical study, *IEEE Transactions on Visualization and Computer Graphics* (2021) 1.
- [8] X. Wei, B. Cao, S. Y. Philip, Unsupervised feature selection on networks: a generative view, in: *Thirtieth AAAI Conference on Artificial Intelligence*, 2016.
- [9] X. Li, C. Wu, P. Li, Ivfs: Simple and efficient feature selection for high dimensional topology preservation, in: *AAAI*, volume 34, 2020, pp. 4747–4754.
- [10] A. Abid, M. F. Balin, J. Zou, Concrete autoencoders: Differentiable feature selection and reconstruction, in: *ICML*, Long Beach, California, United States, 2020, pp. 444–453.
- [11] X. Wu, Q. Cheng, Fractal autoencoders for feature selection, in: *National Conference on Artificial Intelligence*, 2021.
- [12] F. W. Townes, S. C. Hicks, M. J. Aryee, R. A. Irizarry, Feature selection and dimension reduction for single-cell rna-seq based on a multinomial model, *Genome biology* 20 (2019) 1–16.
- [13] M. D. Luecken, F. J. Theis, Current best practices in single-cell rna-seq analysis: a tutorial., *Molecular Systems Biology* 15 (2019).
- [14] M. Belkin, P. Niyogi, Laplacian eigenmaps for dimensionality reduction and data representation, *Neural computation* 15 (2003) 1373–1396.
- [15] C. Fefferman, S. Mitter, H. Narayanan, Testing the manifold hypothesis, *Journal of American Mathematical Society* 29 (2016) 983–1049.
- [16] J. B. Tenenbaum, V. De Silva, J. C. Langford, A global geometric framework for nonlinear dimensionality reduction, *science* 290 (2000) 2319–2323.
- [17] S. T. Roweis, L. K. Saul, Nonlinear dimensionality reduction by locally linear embedding, *science* 290 (2000) 2323–2326.
- [18] D. L. Donoho, C. Grimes, Hessian eigenmaps: Locally linear embedding techniques for high-dimensional data, *Proceedings of the National Academy of Sciences* 100 (2003) 5591–5596.
- [19] Z. Zhang, J. Wang, Mlle: Modified locally linear embedding using multiple weights, in: *Advances in Neural Information Processing systems*, 2007, pp. 1593–1600.
- [20] L. v. d. Maaten, G. Hinton, Visualizing data using t-sne, *Journal of machine learning research* 9 (2008) 2579–2605.
- [21] L. McInnes, J. Healy, J. Melville, Umap: Uniform manifold approximation and projection for dimension reduction, *arXiv preprint arXiv:1802.03426* (2018).
- [22] J. Cook, I. Sutskever, A. Mnih, G. Hinton, Visualizing similarity data with a mixture of maps, in: *In AI and Statistics*, 2007. Society for Artificial Intelligence and Statistics, 2007.
- [23] M. Moor, M. Horn, B. Rieck, K. Borgwardt, Topological autoencoders, 2021. [arXiv:1906.00722](https://arxiv.org/abs/1906.00722).
- [24] L. Wasserman, Topological Data Analysis, *Annual Review of Statistics and Its Application* 5 (2018) 501–532.
- [25] G. Pai, R. Talmon, A. Bronstein, R. Kimmel, Dimal: Deep isometric manifold learning using sparse geodesic sampling, 2018. [arXiv:1711.06011](https://arxiv.org/abs/1711.06011).
- [26] S. Aleyani, J. Tang, H. Liu, Feature selection for clustering: A review, *Data Clustering* (2018) 29–60.
- [27] C. Peng, Z. Kang, Y. Hu, J. Cheng, Q. Cheng, Nonnegative matrix factorization with integrated graph and feature learning, *ACM Transactions on Intelligent Systems and Technology (TIST)* 8 (2017) 1–29.
- [28] X. He, D. Cai, P. Niyogi, Laplacian score for feature selection, in: *NeuIPS*, 2006, pp. 507–514.
- [29] Y. Lu, I. Cohen, X. S. Zhou, Q. Tian, Feature selection using principal feature analysis, in: *15th ACM international conference on Multimedia*, 2007, pp. 301–304.
- [30] D. Cai, C. Zhang, X. He, Unsupervised feature selection for multi-cluster data, in: *SIGKDD*, 2010, pp. 333–342.
- [31] Y. Yang, H. T. Shen, Z. Ma, Z. Huang, X. Zhou, L2, 1-norm regularized discriminative feature selection for unsupervised, in: *Twenty-Second International Joint Conference on Artificial Intelligence*, 2011.
- [32] Z. Li, Y. Yang, J. Liu, X. Zhou, H. Lu, Unsupervised feature selection using nonnegative spectral analysis, in: *AAAI*, volume 26, 2012.
- [33] K. Han, Y. Wang, C. Zhang, C. Li, C. Xu, Autoencoder inspired unsupervised feature selection, in: *International Conference on Acoustics, Speech and Signal Processing*, Calgary, Alberta, Canada, 2018, pp. 2941–2945.
- [34] G. Doquet, M. Sebag, Agnostic feature selection, in: *Joint European Conference on Machine Learning and Knowledge Discovery in Databases*, Würzburg, Germany, 2019, pp. 343–358.
- [35] C. J. Maddison, A. Mnih, Y. W. Teh, The concrete distribution: A continuous relaxation of discrete random variables, *arXiv: 1611.00712v3*, <https://arxiv.org/abs/1611.00712> (2017).
- [36] A. T. Marees, H. de Kluiver, S. Stringer, F. Vorspan, E. Curis, C. Marie-Claire, E. M. Derkx, A tutorial on conducting genome-wide association studies: Quality control and statistical analysis., *International Journal of Methods in Psychiatric Research* 27 (2018) 1–10.
- [37] C. Ludwig, L. C. Gillet, G. Rosenberger, S. Amon, B. C. Collins, R. Aebersold, Data independent acquisition based swath-ms for quantitative proteomics: a tutorial, *Molecular Systems Biology* 14 (2018).
- [38] G. Finak, A. McDavid, M. Yajima, J. Deng, V. H. Gersuk, A. K. Shalek, C. K. Slichter, H. W. Miller, M. J. McElrath, M. Prlic, P. S. Linsley, R. Gottardo, Mast: a flexible statistical framework for assessing transcriptional changes and characterizing heterogeneity in single-cell rna sequencing data, *Genome Biology* 16 (2015) 278–278.
- [39] E. Becht, L. McInnes, J. Healy, C.-A. Dutertre, I. W. H. Kwok, L. G. Ng, F. Ginhoux, E. W. Newell, Dimensionality reduction for visualizing single-cell data using UMAP, *Nature Biotechnology* 37 (2019) 38–44.
- [40] Z. Zang, S. Li, D. Wu, J. Guo, Y. Xu, S. Z. Li, Unsupervised deep manifold attributed graph embedding, *arXiv preprint arXiv:2104.13048* (2021).
- [41] D. Kobak, G. C. Linderman, UMAP does not preserve global structure any better than t-SNE when using the same initialization, *preprint, Bioinformatics*, 2019. URL: <http://biomedrxiv.org/lookup/doi/10.1101/2019.12.19.877522>. doi:10.1101/2019.12.19.877522.
- [42] C. Shorten, T. M. Khoshgoftaar, A survey on image data augmentation for deep learning, *Journal of Big Data* 6 (2019) 1–48.
- [43] S. Z. Li, Z. Zang, L. Wu, Deep Manifold Transformation for Dimension Reduction, *arXiv* (2020). ArXiv: 2010.14831.
- [44] D. Cai, C. Zhang, X. He, Unsupervised feature selection for multi-cluster data, in: *KDD '10*, ACM Press, Washington, DC, USA, 2010, p. 333. URL: <http://dl.acm.org/citation.cfm?doid=1835804.1835848>.

doi:10.1145/1835804.1835848.

- [45] Z. Li, Y. Yang, J. Liu, X. Zhou, H. Lu, Unsupervised Feature Selection Using Nonnegative Spectral Analysis, arXiv (2012) 7.
- [46] X. Wu, Q. Cheng, Q. Cheng, Fractal autoencoders for feature selection, AAAI 35 (2021) 10370–10378.
- [47] Z. Ata., G. Sokar, T. van der Lee, E. Mocanu, D. C. Mocanu, R. Veldhuis, M. Pechenizkiy, Quick and robust feature selection: the strength of energy-efficient sparse training for autoencoders, Machine Learning (2021) 1–38.
- [48] D. Kobak, P. Berens, The art of using t-sne for single-cell transcriptomics, Nature communications 10 (2019) 1–14.
- [49] A. F. Duque, S. Morin, G. Wolf, K. Moon, Extendable and invertible manifold learning with geometry regularized autoencoders, in: Big Data, IEEE, 2020, pp. 5027–5036.
- [50] B. Szubert, J. E. Cole, C. Monaco, I. Drozdov, Structure-preserving visualisation of high dimensional single-cell datasets, Scientific Reports 9 (2019) 8914.
- [51] T. Sainburg, L. McInnes, T. Q. Gentner, Parametric umap embeddings for representation and semisupervised learning, Neural Computation 33 (2021) 2881–2907.
- [52] I. Loshchilov, F. Hutter, Decoupled weight decay regularization, arXiv preprint arXiv:1711.05101 (2017).
- [53] S. Liang, V. Mohanty, J. Dou, Q. Miao, Y. Huang, M. Müftüo, L. Ding, W. Peng, K. Chen, Single-Cell Manifold Preserving Feature Selection (SCMER), Nature Computational Science (2021) 39.